Pure Appl. Geophys.

https://doi.org/10.1007/s00024-025-03903-y

Pure and Applied Geophysics

Sensor Differences of Dual Sphere Superconducting Gravimeters

Clara Beck,[1] Thomas Forbriger,[2,3] and Nico Sneeuw[1]

Abstract—We analyse the difference signal of dual sphere superconducting gravimeters (SG) to identify systematic instrumental disturbances, which would otherwise go unnoticed. Compared to classical spring gravimeters, SGs excel by their superior long-term stability. However, SG measurements also suffer from systematic errors. One possibility for characterising and quantifying these errors is the analysis of sensor differences, either of dual sphere instruments or between two colocated instruments. For perfect instruments, the sensor difference should vanish. We study the sensor differences of all dual sphere SGs in the database of the International Geodynamics and Earth Tide Service (IGETS). As expected, they show a relative drift between the sensors and steps related to operator interventions. However, we can also identify periods of unexpected drift rate changes that last for several months. Afterwards, the drift rate returns to its old value. The observed differences are too big to be caused by local gravity gradients. Therefore, we think, they indicate more complex systematic disturbances of SGs. These disturbances are at the level of a few tens of nm/s^2 and could not be clearly identified in the gravity residuals of only one sensor. These findings are corroborated by the analysis of differences between colocated single sphere SGs at the J9 observatory in Strasbourg. Knowledge of the characteristics and size of these disturbances is important if gravity changes of a few tens of nm/s^2 are studied on long time scales, like signals from hydrology or polar motion.

Keywords: Superconducting gravimeter, sensor difference, instrumental disturbances, drift.

1. Introduction

Studying how gravity changes over time gives us more insights about Earth. This ranges from information about its deep interior, like the properties of mantle material, to better knowledge about processes at the surface, like hydrological mass transport. An overview of the measurement methods and applications of time variable gravity at the Earth's surface is given by Crossley et al. (2013).

One type of instrument to measure the temporal gravity variations on the Earth's surface is superconducting gravimeters (SGs). They outperform classical spring gravimeters in terms of long-term stability. Their drift behaviour is mainly linear and a few hundred times smaller than the typical drift of spring gravimeters (Crossley et al., 2013).

These properties have made SGs a great tool for observing gravity changes, especially on longer timescales where spring gravimeters reach their limits due to their drift properties. Examples are studies of local or regional hydrology (Crossley et al., 2004; Neumeyer et al., 2008; Luan et al., 2023; Kumar et al., 2023; Creutzfeldt et al., 2010), vulcanology (Carbone et al., 2019) or the Earth deformation due to polar motion (Xu et al., 2004; Ziegler et al., 2016; Ding and Chao, 2017).

However, while instrumental disturbances of SGs are much smaller than those of spring gravimeters, they are not negligible. Some known examples are the aforementioned mainly linear drift of up to 110 nm/(s^2 year) (Crossley et al., 2004; Bützler, 2018) and steps up to 5000 nm/s^2. The drift can also show exponential components (Van Camp and Francis, 2007).

Before analysing gravity changes, these instrumental disturbances have to be corrected. The instrumental drift can be determined by regular measurements of absolute gravimeters (AGs) in the immediate vicinity of the SG (Van Camp and Francis, 2007; Wziontek et al., 2009). AG measurements are

[1] Institute of Geodesy, University of Stuttgart, Geschwister-Scholl-Str. 24D, 70174 Stuttgart, Germany. E-mail: clara.beck@gis.uni-stuttgart.de; nico.sneeuw@gis.uni-stuttgart.de

[2] Geophysical Institute, Karlsruhe Institute of Technology (KIT), Hertzstrasse 16, 76187 Karlsruhe, Germany. E-mail: thomas.forbriger@kit.edu

[3] Black Forest Observatory, Karlsruhe Institute of Technology (KIT) and University of Stuttgart, Heubach 206, 77709 Wolfach, Germany.

Published online: 18 March 2026

not affected by the issue of drift but show their own systematic uncertainties.

Several methods exist to correct steps in SG time series (Hinderer et al., 2007, 2002; Van Camp and Vauterin, 2005; Pagiatakis, 2000). Most of them are based on manual inspection. In particular, if a step occurs together with a data gap, or if the data shows a relaxation characteristic after the step, uncertainties remain in the step correction. A comparison of step corrections from four different methods and operators was performed by Hinderer et al. (2002). For the same step and the same data, they found differences of up to 10 nm/s^2 between different step correction methods.

To have better control of instrumental disturbances, especially steps in the data, dual sphere SGs were developed in the late 1990s (Richter, 1998; Hinderer et al., 2007). These SGs have two separate sensors inside the same liquid helium Dewar. One sensor is located 20 cm above the other. Figure 1 shows a conceptual sketch of such an instrument. Today, seven out of 60 SGs in the database of the International Geodynamics and Earth Tide Service (IGETS) (Boy et al., 2023) are dual sphere instruments. However, the gravimeter me073 in Metsahovi was separated into two single sphere SGs only several months after the beginning of the registration due to some instrumental problems (A. Raja-Halli, 2023, pers. comm.). The remaining six dual sphere SGs have operated between 6 and 25 years long. An overview of these instruments can be found in Table 1, and a map of their locations is shown in Fig. 2.

The two sensors of dual sphere SGs are exposed to the same gravity field and should measure the same change in gravity. As SGs are relative gravimeters, any constant component of the measurements is meaningless and can be set to zero. Afterwards, the difference between the measurements of the two sensors should vanish for a perfect instrument. Every signal present in the difference between the measurements of the two sensors is expected to show an instrumental disturbance. We call this difference *sensor difference*. Sensor differences help to detect and analyse instrumental disturbances. However, it has to be carefully considered if the differences might be caused by local gravity gradients.

Kroner et al. (2005) calculated sensor differences for the four dual sphere SGs existing at the time. The resulting time series have a peak-to-peak amplitude of 10 nm/s^2 to 20 nm/s^2 and contain some high-frequency noise and other signals on time scales of months. They discuss a possible correlation with air pressure variations. At that time, less than four years of data were available for the different SGs. Today, data is available for much longer time periods and

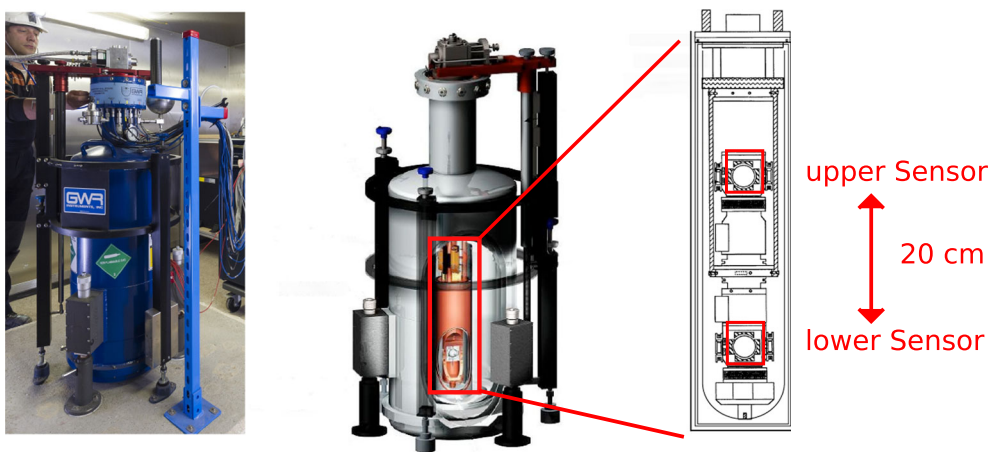

Figure 1
Design of a dual sphere superconducting gravimeter. The figure shows the instrument bf056 at station Schiltach (left)(cropped from a photo by Markus Breig), the design of the Dewar (middle)(adapted from Instruments (2009)) and the gravity sensing unit (right)(adapted from Goodkind (1999))

Table 1

Data of dual sphere SGs. The table gives the time periods and the data sources used in this study

Station	Instrument	Time period	Data source
Schiltach	bf056	2010/07–2024/12	https://doi.org/10.5880/BFO
Bad Homburg	bh030	2001/02–2007/04	https://doi.org/10.5880/igets.bh.l1.001
Moxa	mo034	2001/01–2023/06	IGETS Level 1
Sutherland	su037	2001/01–2006/12	https://doi.org/10.5880/igets.su.l1.001
		2007/12–2008/07	
		2010/01–2017/09	
		2018/01–2023/03	
Wettzell	we029	2000/01–2010/10	https://doi.org/10.5880/igets.we.l1.001
		2012/08–2018/03	
Wettzell	we030	2010/06–2018/03	https://doi.org/10.5880/igets.we.l1.001

two more gravimeters, which allows us to repeat their analysis in much more depth and detail.

A similar analysis can also be done if two or more single sphere SGs are colocated. Such an experiment was done at the J9 observatory in Strasbourg. Between 2016 and 2021, eight different SGs have been operating there, up to five simultaneously. A comparison was published by Hinderer et al. (2022). They found the benefit of relative calibration of colocated instruments compared to absolute calibration with absolute gravimeters. When analysing the drift of the instruments, they found a correlation between the body temperature and the initial exponential drift. Further, they studied the instrumental self noise. Other instrumental effects were not discussed.

Many authors like Creutzfeldt et al. (2010), Kumar et al. (2023) and Luan et al. (2023) have analysed signals from hydrology in SG times series. They are mostly seasonal but not strictly periodic and can reach up to 180 nm/s^2 (Kumar et al., 2023). Often they are smaller, depending on local conditions. For example Luan et al. (2023) studied hydrological signals with an amplitude of 80 nm/s^2 at station Kunming in China. Seasonal signals appear trend-like on time scales of a few months. For this kind of studies, the knowledge of instrumental disturbances on the same time scales is of major importance to avoid misinterpretation of instrumental disturbances as geophysical signals.

Another field of study where small instrumental disturbances of SGs on time scales of months matter is the gravity signal of polar motion. It is a periodic signal with an amplitude of up to 40 nm/s^2 (see for example, Ziegler et al. (2016)).

To gain more insight into instrumental disturbances of SGs, we have computed and analysed the sensor differences of all six dual sphere SGs of the IGETS database. The data processing is described in Sect. 2. The results are presented in Sect. 3. We focus on disturbances happening on time scales longer than a month. In Sect. 4 we discuss the characteristics and possible causes of the observed signals. We further compare them to sensor differences between colocated single sphere SGs at the J9 observatory in Strasbourg. Finally, in Sect. 5 we summarise the results.

2. Data Processing

We use IGETS Level 1 data (see Table 1 for exact data sources) to compute gravity residuals and sensor differences. The different steps of this computation are described in this section.

First, the raw gravity measurements are converted from voltage to gravity, using the calibration factors published together with the Level 1 data or communicated by the operators (instruments bh030, we029 and we030, H. Wziontek, 2025, pers. comm.). Time shifts between the two sensors are smaller than 2 s. This leads to differences between the output of the two sensors smaller than gravity changes occurring within 2 s. They are insignificant compared to the

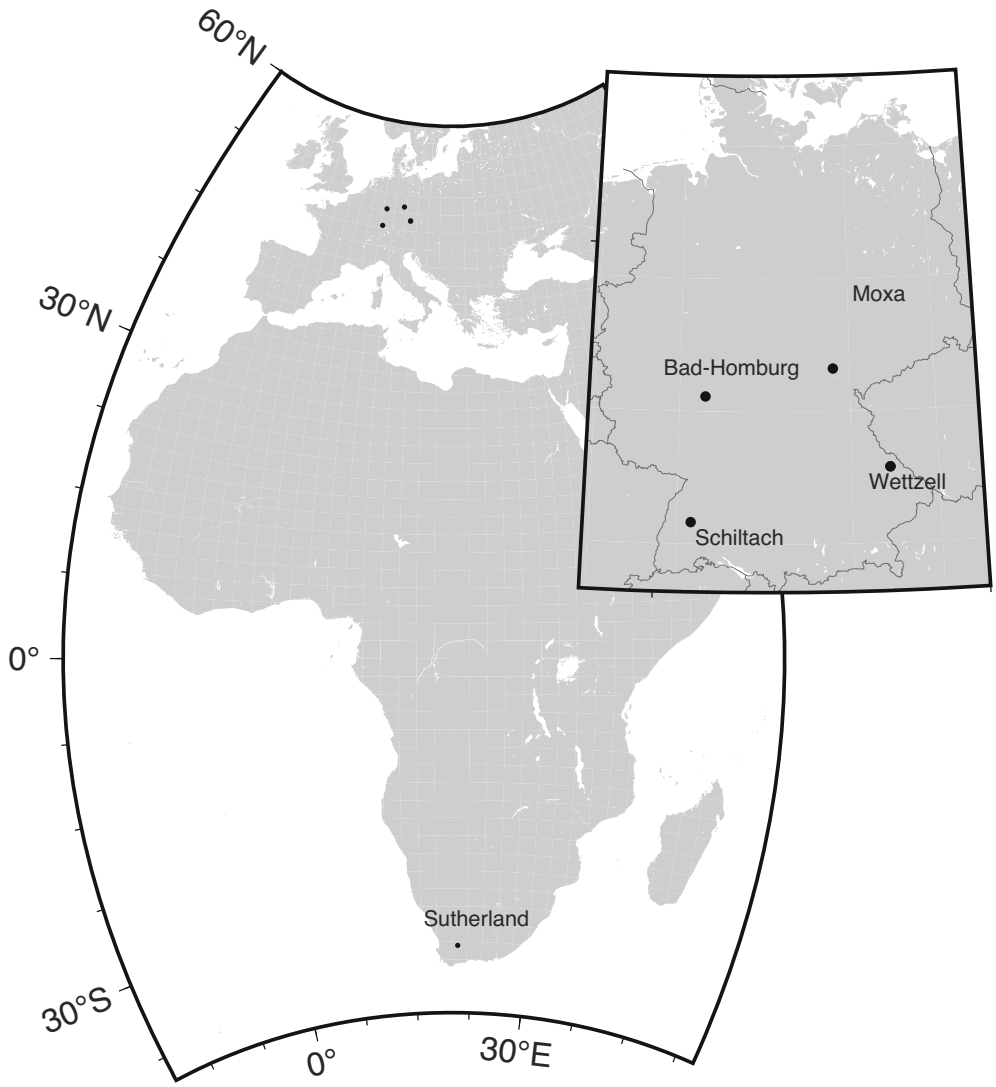

Figure 2
Location of dual sphere superconducting gravimeters

other signals we observe in the sensor differences. Therefore, time lags are ignored in this study. Some time periods with obviously corrupted data are excluded. Examples for this are constant gravity output or truncated tides due to saturation of the output voltage.

The major contributions to the gravity signal, i.e. tides, polar motion and gravity change due to air pressure variations, are removed by corrections.

For the tidal correction, a local model is used. At the stations Bad Homburg, Wettzell, Sutherland and Moxa, the local model is taken from IGETS Level 3 data (Boy, 2022). These models use tidal parameters obtained by tidal analysis for diurnal and sub-diurnal bands and a DDW99 (Dehant et al., 1999) model for longer periods. For station Schiltach, we use the tidal parameters from tidal analysis (E. Schroth, 2018, pers. comm.) for wave group MM (signal period ranging from 47.88 d to 18.27 d, including the lunar monthly constituent) and groups of higher frequency. For longer period tides, we use nominal values (1.16 for the gravimetric factor and 0° for the phase lag).

We could also use the local model from the IGETS data for BFO, but at this station we have more experience with our own model. At each station, a gravimetric factor of 1.16 and a phase lag of 0° is assumed for polar motion.

We apply a local air pressure correction with the nominal admittance factor of −3 nm/(s^{2}hPa) (Crossley et al., 2013) for all sensors. Kroner et al. (2005) found differences in the regression coefficients between local air pressure and gravity for the upper and the lower sensor of dual sphere SGs of up to 0.1 nm/(s^{2}hPa). However, as they mention, these differences are too big to be related to a height dependence of atmospheric gravity changes. Therefore, we think applying the same pressure admittance factor for both sensors is more reasonable. Applying different admittance factors would hide instrumental or other effects into a pseudo-atmospheric effect. In Sect. 4.3, we will investigate a possible remaining relationship between sensor differences and air pressure changes.

Outliers are rejected from the gravity residuals if they differ from the median in a one-week window of more than five scaled median absolute deviations. For a detailed description, see Appendix A.

As discussed above, the removal of steps is a critical part of computing gravity residuals. Here, we manually determine the epochs of steps greater than 10 nm/s^2 in the data of each sensor. As heavy rain events can have a step-like gravity response, it might happen that we wrongly identify such events as instrumental steps. We try to avoid this by visually inspecting the characteristic of the steps (simultaneous data gaps, time length of the step). The number of steps for each sensor is reported in Table 2. Afterwards, we remove them with the following procedure:

- We extract the data three weeks before and after the step.
- We model this data by

$$g^{\mathrm{res}}(t) = at + b + cH(t - t_0)\,,$$

where $g^{\mathrm{res}}(t)$ are the gravity residuals as a function of time, t_0 is the time of the step, and a, b and c are regression coefficients to estimate with a linear least-squares approach. The step is parametrised by the Heaviside function

$$H(t) = \begin{cases} 0 & \text{for } t \le t_0 \\ 1 & \text{for } t > t_0\,. \end{cases}$$

- The estimated coefficient c is the size of the step. This constant is removed from all data points after the step.

As there often occurs relaxation after the steps, we do not use the first 6 h after the step for the estimation. If the time between two steps is shorter than three weeks, the time span of the least-squares adjustment is shortened accordingly. This procedure is probably not the best for each step. Especially, the best time span for the adjustment might be different for different steps and depends on the size of the step, the duration of possible data outage at the epoch of the step, the length of relaxation behaviour after the step and the characteristics of the residuals, among others. Here, we have chosen a three weeks window before and after the step by testing different window length and visually evaluating the success of the step corrections. In particular, in the case of major disturbances like power outages, it is important to choose a time window that is long enough to avoid

Table 2

Number of corrected steps

Station	Sensor	Time period	#
Schiltach	bf056-1	2010/07–2024/12	10
Schiltach	bf056-2	2010/07–2024/12	11
Bad Homburg	bh030-1	2001/02–2007/04	28
	bh030-2	2001/02–2007/04	28
Moxa	mo034-1	2001/01–2023/06	21
Moxa	mo034-2	2001/01–2023/06	32
Sutherland	su037-2	2001/01–2006/12	4
		2007/12–2008/07	5
		2010/01–2017/09	10
		2018/01–2023/03	9
Sutherland	su037-2	2001/01–2006/12	4
		2007/12–2008/07	4
		2010/01–2017/09	11
		2018/01–2023/03	10
Wettzell	we029-1	2000/01–2010/10	45
		2012/08–2018/03	4
	we029-2	2000/01–2010/10	41
		2012/08–2018/03	7
Wettzell	we030-1	2010/06–2018/03	19
Wettzell	we030-2	2010/06–2018/03	18

Table 3

Removal of a linear trend

Station	Instrument	Time period	Time period used for estimating a linear trend	Trend in nm/(s^2 year)	
				Lower sensor	Upper sensor
Schiltach	bf056	2010/07–2024/12	2019/09/01–2024/12/31	−3.79	103.02
Bad Homburg	bh030	2001/02–2007/04	no trend removed	–	–
Moxa	mo034	2001/01–2023/06	2006/01/01–2013/12/31	35.81	20.45
Sutherland	su037	2001/01–2006/12	full data	26.88	23.45
		2007/12–2008/07	no trend removed	–	–
		2010/01–2017/09	2014/07/09–2017/09/22	1.80	140.46
		2018/01–2023/03	2019/08/17–2020/10/27	0.45	136.71
Wettzell	we029	2000/01–2010/10	no trend removed	–	–
		2012/08–2018/03	2014/11/12–2017/09/04	98.19	45.76
Wettzell	we030	2010/06–2018/03	2015/02/20–2018/02/19	122.08	24.53

too many influences on the linear adjustment by disturbances occurring together with the step. On the other hand, the time window should not be too long so that modelling the gravity change as a linear trend is justified. Bützler (2018) has tested different time spans between half a month and one year to adjust the step sizes for the instrument bf056. She found differences in the estimated step size of up to 40 nm/s^2 for one individual step. We will discuss later in how far the weak points of our step correction (e.g. possible classification of rain events as instrumental disturbance, imperfect window length for the adjustment) might affect our results.

After the step correction, a possible linear trend is removed from the residuals. The trend is estimated by a linear least-squares regression during a time period without major disturbances. These time periods are listed together with the estimated trends in Table 3. The trend can either originate from instrumental drift or show a secular gravity change.

Finally, for each dual sphere SG, we compute the sensor difference

$$g_{\mathrm{diff}}(t) = g^{\mathrm{res}}_{\mathrm{lower}}(t) - g^{\mathrm{res}}_{\mathrm{upper}}(t)$$

from the residuals of the upper and the lower sensor $g^{\mathrm{res}}_{\mathrm{upper}}(t)$ and $g^{\mathrm{res}}_{\mathrm{lower}}(t)$.

3. Results

Figure 3 shows the sensor differences of all six dual sphere SGs. Besides some remaining outliers, their peak-to-peak amplitude is between 70 nm/s^2 (bh030) and 155 nm/s^2 (bf056). The signals consist mainly of

a) remaining steps, that were not corrected because they are smaller than 10 nm/s^2 or not perfectly corrected due to uncertainties in the step correction,
b) a relaxation component of the drift, which might be modelled as an exponential function with a negative exponent, appearing not only at the beginning of the registration but also after major interventions like the reinitialisation after replacing the Dewar for we029 in 2012; the annealing process during this reinitialisation was difficult to control since a temperature sensor inside the vacuum can is missing in the old sensors; this temperature sensor is normally used during the initialisation with the new Dewar (H. Wziontek, 2024, pers. comm.),
c) high-frequency disturbances, for example, remaining outliers, that were not detected by our outlier rejection procedure,
d) small tidal remainders with an amplitude of up to 3 nm/s^2, which indicate uncertainties in the calibration factors,
e) and changes in drift rates on time scales of several months.

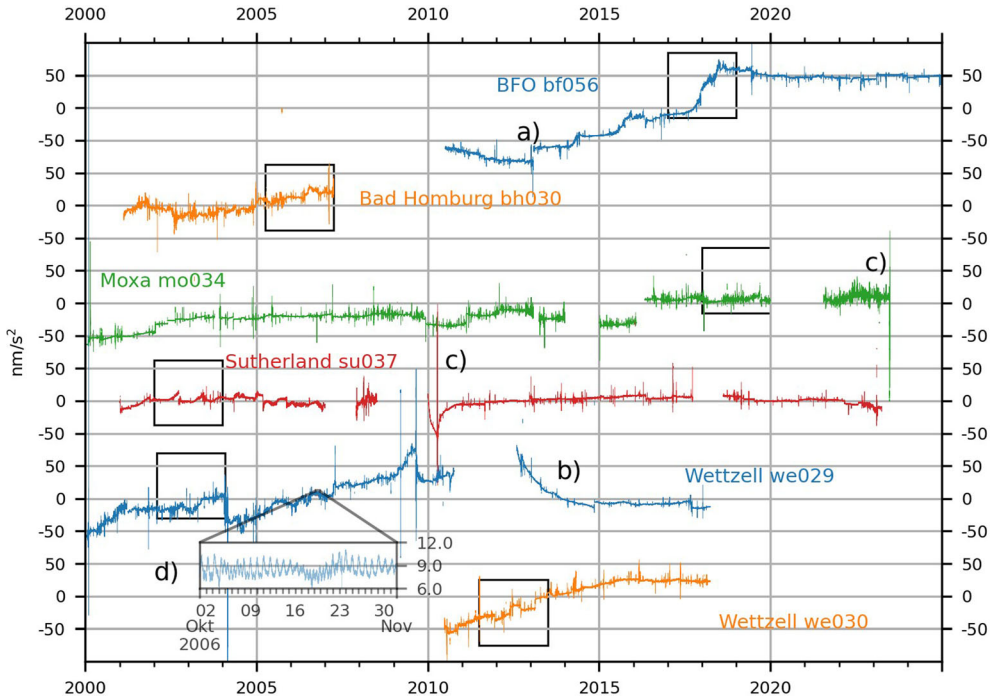

Figure 3

Sensor differences. The figure shows the resulting sensor differences after removing steps, outliers and linear trends. Remaining outliers that exceed 150 nm/s^2 are excluded. Offsets are adjusted for illustration purposes. **a**–**d** show examples of the different types of signals present in the sensor difference, discussed in the text. A closer view of the time windows marked with a rectangle can be found in Fig. 4

Examples of a)–d) are marked in Fig. 3, examples of e) can be found for each dual sphere instrument and are shown in Fig. 4. The drift rate changes are beyond the known types of instrumental disturbances discussed in the introduction, like linear or exponential drift and steps. To ensure they are not an artefact of our data processing, for example, the imperfect step correction, we also calculate sensor differences from IGETS Level 2 products processed by EOST (École et observatoire des sciences de la terre). Boy (2022) describes the processing from IGETS Level 1 data to IGETS Level 2 data. It corrects instrumental disturbances like steps and outliers. For Moxa we additionally compute the sensor difference for a data set provided by the operators after outlier and step correction (T. Jahr, 2022, pers. comm.). The results are shown in Appendix B. The remaining steps and the presence of high-frequency noise differ between the sensor differences computed from different data sets. There are more transient disturbances in the sensor differences computed from IGETS Level 2 data than in the sensor differences computed with our own corrections from IGETS Level 1 data. However, the drift rate changes remain unchanged for all data sets. Further, an imperfect step correction can only cause steps in the sensor difference, but not changes in drift rates.

4. Discussion

The results presented in the previous section lead to the following questions:

1. How can we characterise the drift rate changes?
2. Might they originate from actual gravity gradients?
3. Can we relate these signals to other instrumental or environmental parameters?

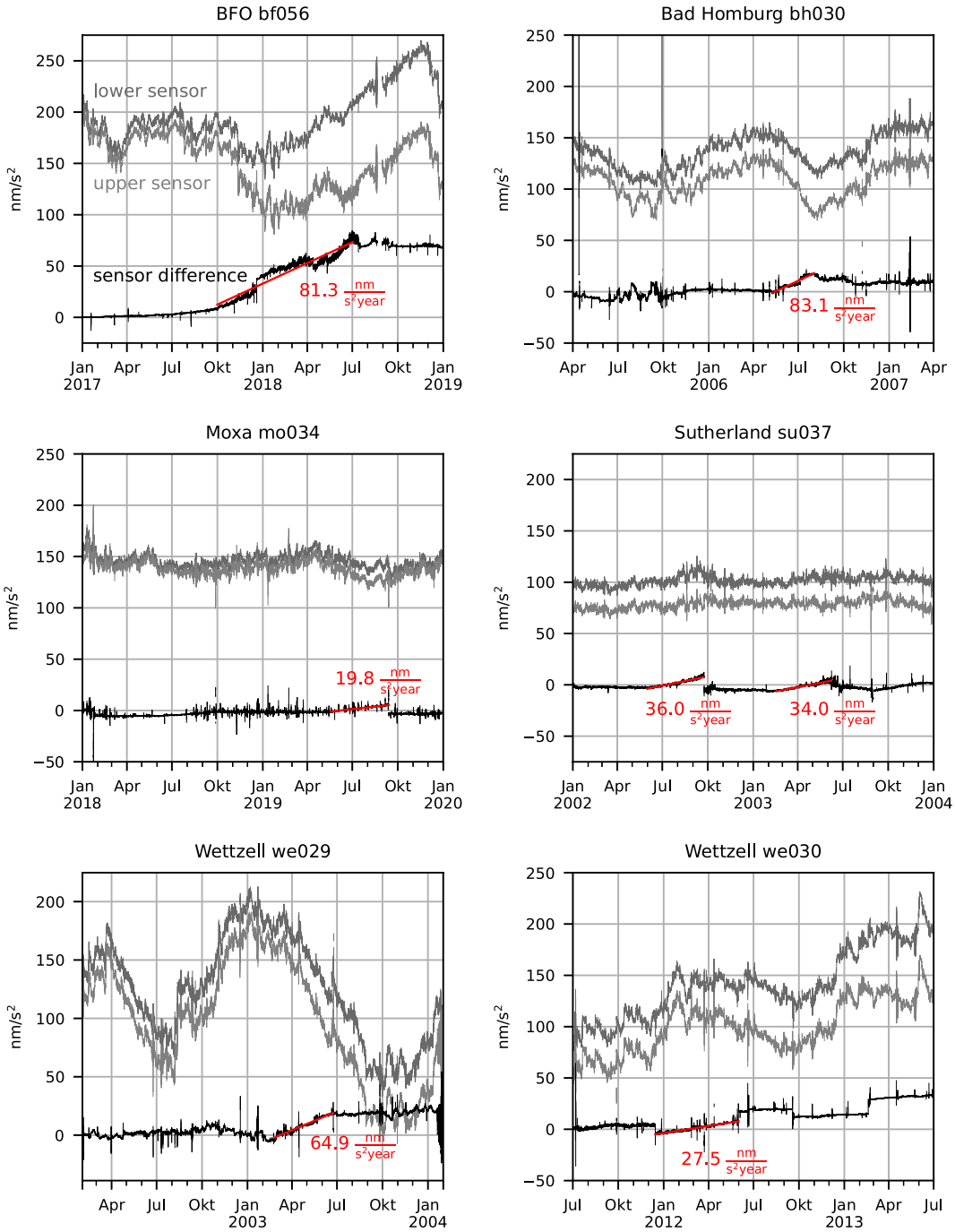

Figure 4
Examples of drift rate changes in sensor differences. For each dual sphere sensor, examples of time periods with drift rate changes in the sensor difference are shown (black). Further, we show the gravity residuals of the two sensors (dark and light grey). Offsets are adjusted for illustration purposes

4. Are these signals specific to dual sphere instruments, or can we find similar signals in differences of colocated instruments?

We will discuss these questions in this section.

4.1. *How Can We Characterise the Drift Rate Changes?*

From Figs. 3 and 4 we find the following properties of the drift rate changes: The rate change is between 20 nm/(s^{2}year) and 83 nm/(s^{2}year). The changed drift value remains for several months. Afterwards, the drift returns to its previous value. While for some examples (bh030, we029) the apparent drift rate change consists of several small subsequent steps, this is not the case for other examples (bf056, we030, su037, mo034), where a real change of the linear trend occurs. The cumulative signal of one drift rate change is between 5 nm/s^2 and 60 nm/s^2 for the shown examples. For all examples we could find, the drift rate change in the sensor difference is positive. Further, for all examples besides the one at bh030 the return to the old drift value coincides with a step. For the instruments bf056, mo034, we029 and we030, such a step was already adjusted in one or both sensors by our step correction procedure. Especially, for the instruments mo034, su037 and we030, a step is still visible at the end of the drift rate change in the sensor difference (Figs. 3, 4). However, these remaining steps cannot be clearly identified in the gravity residuals, and they can hardly be assigned to one sensor. Operator interventions that might be related to these steps are discussed in Appendix F.

Likewise, the changes in drift rates cannot be identified in the data of one single sensor. The data from one single sensor does not appear suspicious. So, the data from the second sensor is needed to identify the disturbances. Further, we need to consider half of the observed sensor difference as a lower bound for the disturbance of at least one sensor. Common mode disturbances can be much bigger as they cancel out in the sensor difference.

The cumulative signal of one drift rate change is on the same order of magnitude as the gravity residuals themselves. This can lead to misinterpretation of the gravity residuals. We illustrate this with the example of the instrument bf056 shown in Fig. 4. Both sensors show a gravity decrease in autumn 2017, followed by a gravity increase in spring and summer 2018. This could be interpreted as a hydrological mass movement: In autumn, rain accumulates in the soil. As Schiltach is an underground station, this leads to a gravity decrease. In spring and summer, the soil dries out again, and gravity increases. However, the apparent size of the gravity decrease and increase is different for the two sensors. While the lower sensor sees a small gravity decrease of 25 nm/s^2 followed by a large gravity increase of 100 nm/s^2, the upper sensor sees a gravity decrease and increase both of the same size of 75 nm/s^2. The difference is expressed by the sensor difference. With a single sphere sensor, we would not be aware of the large uncertainty of the hydrological signal.

4.2. *Might the Drift Rate Changes in Sensor Differences Originate from Actual Gravity Gradients?*

As the two sensors of a dual sphere SG are vertically separated by 20 cm, such an instrument could theoretically act as a gravity gradiometer and measure the vertical gravity gradient. Therefore, we analyse if the observed drift rate changes can originate from a local mass redistribution.

First, we reproduce an increasing sensor difference with a body in the vicinity of the gravimeter, whose density slowly increases during a few months. The body could, for instance, represent a volume that is slowly saturated with water. After the complete emergence, the mass should lead to a gravity difference of about 20 nm/s^2 between the two sensors. We choose 20 nm/s^2 as a representative value of the cumulative signal of one drift rate change (see Sect. 4.1 and Fig. 4). Further, we calculate the total gravity effect of this mass. Only if this total gravity change would be too small to be detected, or if it indeed is present in the gravity data along with the expected change in gravity gradient, the local mass can explain the drift rate changes in the sensor difference.

As a simplified model for the mass, we use a cylinder placed below the gravimeter whose axis coincides with the sensor axis. This cylinder could, for example, represent cumulative water in the soil originating from rainfall or another local hydrological effect. For cylinders of different height (between 1 cm and 100 m) and radius (between 1 cm and 1 km), we vary the distance to the gravimeter and calculate the density needed to produce a gravity difference of 20 nm/s^2 between the two sensors. The exact geometry of the cylinder and the calculation are presented in Appendix C. For cylinders with a radius $r < 1$m, the required density change quickly reaches values much higher than the density of water when the distance to the gravity sensors increases. The only test cases for which realistic changes in density ($\leq$ the density of water) result in a sensor difference of 20 nm/s^2 and gravity changes on the observed order of magnitude ($\leq 200 nm/s^2$, see Fig. 3) are cylinders with a radius of 1 m or 2 m and a height of at least 1 m (see Fig. 12). However, also in these cases, the cylinder has to be very close to the gravimeter ($h < 1$m). Further, it is difficult to find a corresponding natural process, where, for example a cylinder with a radius of 2 m and a height of 10 m gets saturated with water, while the soil outside the cylinder remains dry. It would be more realistic that a larger area gets saturated. However, for all tested cylinders with a radius larger than 2 m the corresponding gravity change at the lower sensor gets significantly larger than the observed variations of the gravity residuals. Even if these models are highly simplified, they show that it is hard to find a geophysical mass change that could produce the observed changes in the gravity gradient. If it exists, it needs to be very local and localized.

A comparison with geophysical gravity gradients observed with vertically separated SGs gives more insights: As an example, we use the results from the low background noise interdisciplinary ground and underground-based research laboratory (LSBB). There are two SGs installed inside an active karst system: the iOSG24 underground and the iGrav31 at the surface (Kumar et al., 2023). They are separated by 520 m. Due to the complex hydrology of the karst system, we expect large mass movement in the vicinity of the gravimeters, leading to comparably large gravity gradients. The amplitude of the difference signal of the two instruments is about 200 nm/s^2 (Kumar et al., 2023). The corresponding change in gravity gradient is 0.38 nm/(s^{2}m). We would expect the gravity gradients at the stations of the dual sphere instruments to be at most at the same order of magnitude as at LSBB. However, an observed change in sensor differences of about 20 nm/s^2 leads to a change in gravity gradient of 1×10^3 nm/(s^{2}m) for sensors separated by 20 cm. That is 2000 times the gravity gradient observed at LSBB. This indicates that the drift rate changes in the sensor differences are very unlikely originating from local hydrology.

The third reason for expecting the observed drift rate changes to show instrumental disturbances rather than changes in the local gravity gradient is the sign of the drift rate changes: For all the examples we could find, they are positive. For an effect of local hydrology, we would expect a different sign for underground stations (Schiltach and Moxa) than for surface stations (Bad Homburg, Wettzell and Sutherland).

4.3. *Can We Relate These Signals to Other Instrumental or Environmental Parameters?*

We expect the observed drift rate changes are not caused by changing gravity gradients but by unknown instrumental disturbances. In this section, we examine if we can find a correlation or coincidence between the drift rate changes and other environmental or instrumental parameters or interventions by the operators.

For the instrument su037 in Sutherland Kroner et al. (2005) found an amplitude reduction of the sensor difference when applying different pressure admittance factors for the two sensors. However, they further discuss that the differences are too big to be explained by a true height dependence of atmospheric gravity changes. Therefore, as discussed in Sect. 2, we apply the same pressure admittance factor for both sensors to avoid hiding an instrumental effect into a pseudo-atmospheric effect. To analyse a remaining possible correlation between air pressure and sensor differences, examples of drift rate changes in sensor differences are shown together with the air

pressure signal in Fig. 5. We cannot find a systematic correlation.

Figure 6 shows two examples of drift rate changes in the sensor difference of the instrument bf056 at Black Forest Observatory (BFO, Station Schiltach) together with other environmental and instrumental parameters: the liquid helium level inside the Dewar, the room temperature, the air humidity, upper and lower neck temperature of the cold head, the current in the Dewar heater and the heater current at the gravity sensing unit.

One instrumental parameter, which might directly cause a changing gravity gradient, is the liquid helium level. In Appendix D we show that the gravitational attraction of a varying liquid helium level can lead to changes of up to 10.5 nm/s^2 in the sensor difference. However, a change in liquid helium level of 20 % to 51 % would be needed. During the time of drift rate changes at BFO, the liquid helium level only fluctuates by a few percent (see Fig. 6). Thus, variations of liquid helium cannot be responsible for the drift rate changes of bf056. Nevertheless, we cannot exclude this for all other sensors, where liquid helium level variations might be larger, especially for the older Dewars that require regular helium refill.

From the other environmental and instrumental signals shown in Fig. 6, only the upper neck temperature shows a consistent correlation with the sensor differences for both examples of drift rate changes. However, we should interpret this correlation with caution as any trend-like signal correlates with any other trend-like signal. Further analysis would be needed to test whether this is a random coincidence or if it implies causality.

Hinderer et al. (2022) found a correlation between the linear or exponential sensor drift and the body temperature for several SGs in Strasbourg. They conclude that the absorption of helium out of the vacuum can of the sensor and resulting changes of mass or thermal gradients might be sources of drift. Similar effects could also be possible reasons for the drift changes we observe for the dual sphere SGs. Unfortunately, we cannot include the body temperature to the comparison in Fig. 6 as the body temperature inside the instrument bf056 is not measured continuously. It was only measured during initialisation.

The tilt of the instrument bf056 at BFO is special compared to other SGs. As the observation point is known to be very stable in terms of tilts, the operators decided to turn off the tilt compensation system. Further, the tiltmeters are damaged. As bf056 is the only dual sphere SG, which is not tilt stabilised and shows the largest drift rate change signals in the sensor difference, one could speculate that the drift rate changes are related to tilt. As the sensitive axis of the two sensors of a dual sphere SG are not exactly parallel even if the tilt compensation is turned on for the lower sensors, the upper sensor can still be tilted. At bf056, manual measurements of the vertical alignment of the two sensors were performed in January 2013 and September 2020. A description of these tests and the results can be found in Appendix E. Between these two measurements the the vertical alignment of the lower sensor changed by -20.1 ± 2.1 µrad and 1.65 ± 0.12 µrad for the two orthogonal directions and the vertical alignment of the upper sensor changed by -23.8 ± 4.0 µrad and 2.6 ± 1.8 µrad. The main reason for changes in the vertical alignment is tilt changes of the whole instrument. Such tilt changes cause the same change in the vertical alignment for both sensors. However, the changes in the vertical alignment could be slightly different for the two sensors if other effects are involved. Examples are small deformations inside the sensor or movements of the spheres within the magnetic field. The supporting magnetic field itself gets distorted by the niobium cylinder and might not be perfectly symmetric to the axis of the cylinder. The observed changes in the vertical alignment lead to a change of 12 nm/s^2 in the sensor difference (see Appendix E). This is only one tenth of the observed change in the sensor difference during the same time. The size of the observed change in sensor difference over seven years depends greatly on the trend removed from each sensor. Nevertheless, we conclude from the different magnitudes that the drift rate changes are likely not caused by tilt changes.

Furthermore, we search for coincidences between operator interventions and drift rate changes. For none of the six instruments, we can find a clear coincidence between operator interventions and the

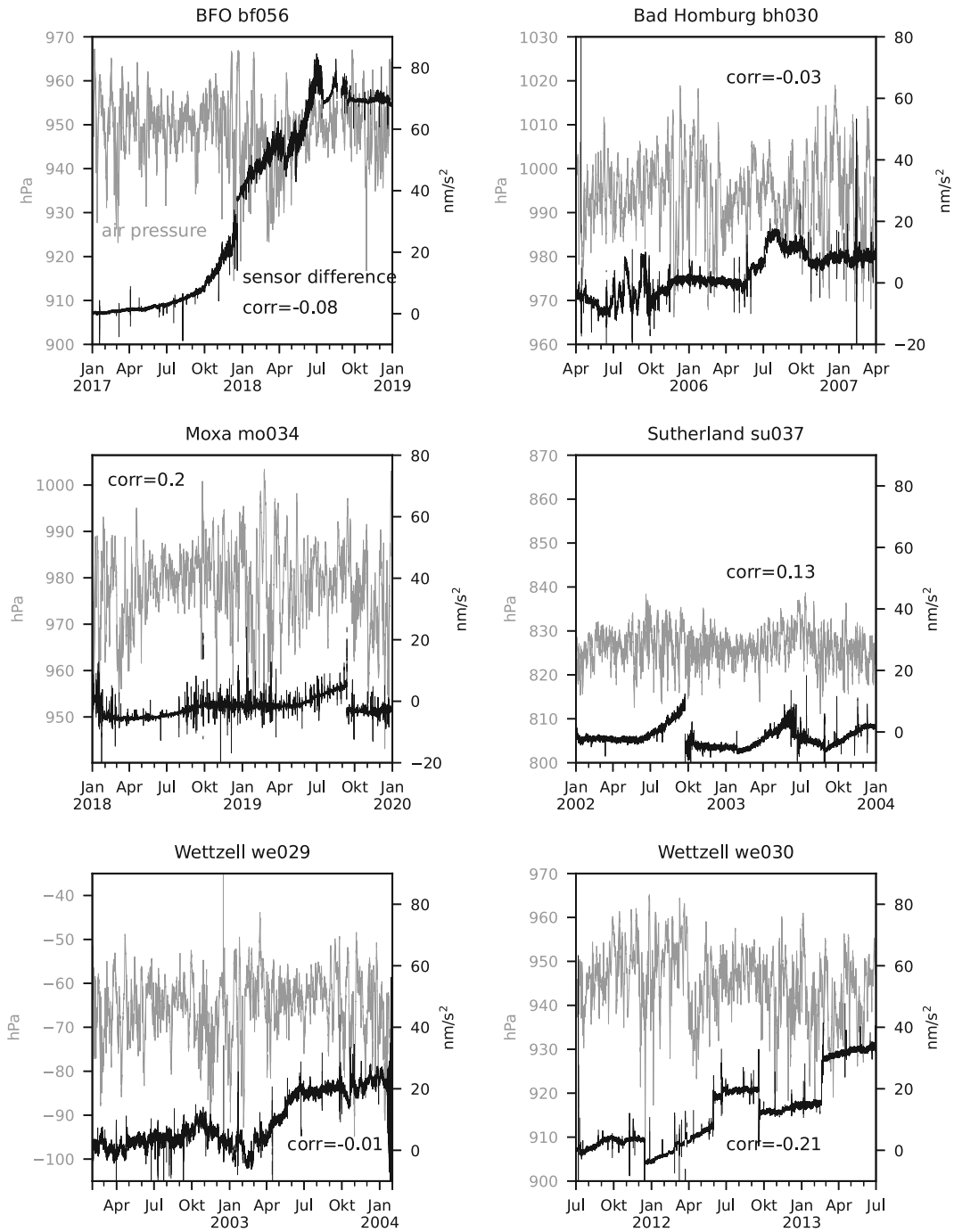

Figure 5
Sensor differences and air pressure variations. The figure shows the same time windows as in Fig. 4. Sensor differences are shown in black, and air pressure variations are in grey. We indicate the Pearson correlation coefficients between air pressure and sensor difference in the shown time period

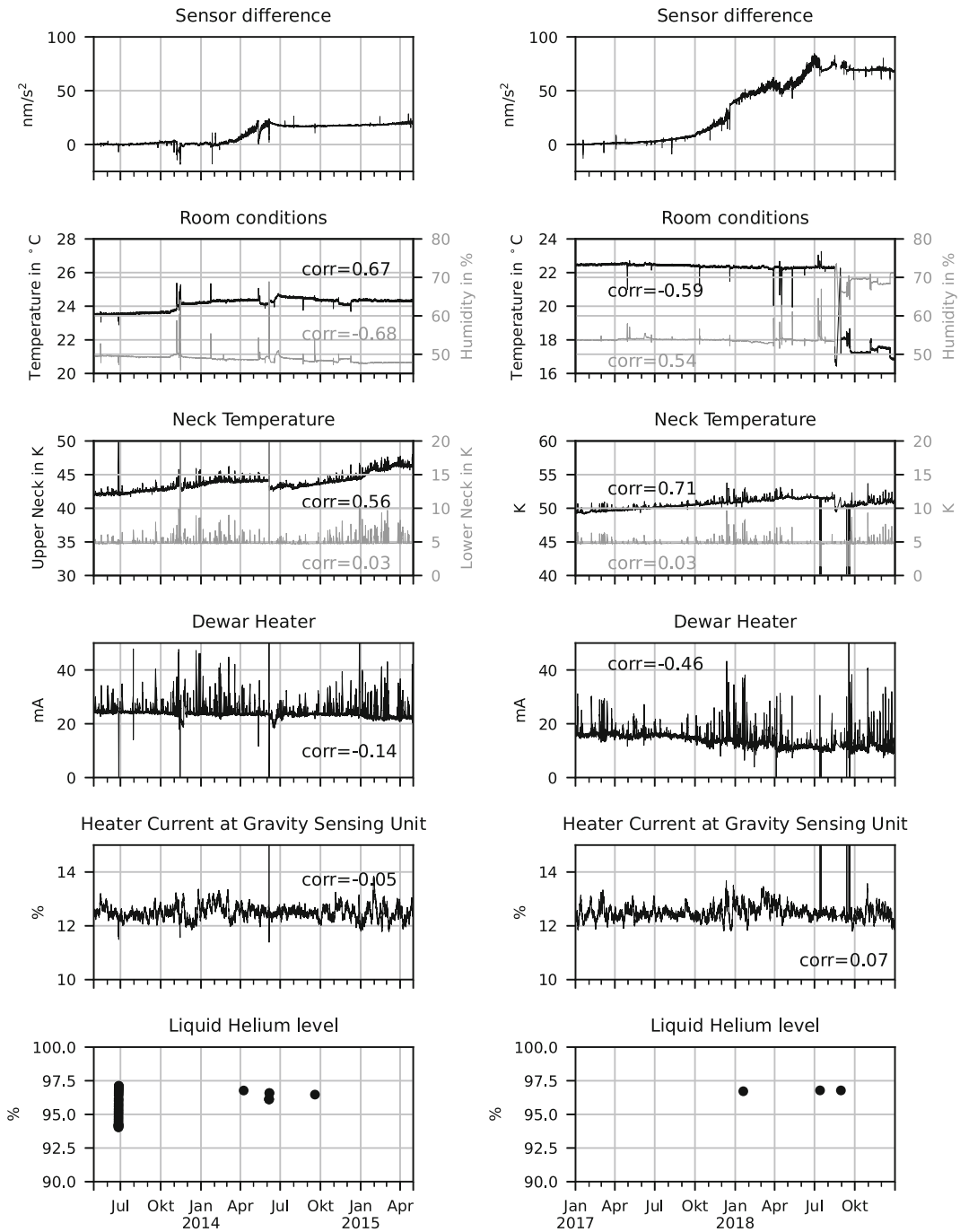

Figure 6

Sensor differences and environmental and instrumental parameters. The figure shows two examples of drift rate changes in the sensor difference of bf056. Additionally, we show a variety of instrumental and environmental parameters. The Pearson correlation coefficients between the sensor difference and the environmental and instrumental parameters are indicated for the corresponding time period

onset of drift rate changes, while the return to the old drift value coincides with a step and an operator intervention for the instruments bf056, mo037, su037 and we029 and with a step without an operator's intervention for the instrument we030. At least at BFO, the drift rate changes were not the reason for

the maintenance actions. More details about operator interventions during time periods of changed drift rate can be found in Appendix F.

4.4. *Are These Signals Specific to Dual Sphere Instruments, or Can We Find Similar Signals in Differences of Colocated Instruments?*

From analysing sensor differences, we can only find a lower bound for the disturbance of at least one of the sensors. We do not know if the disturbance occurred at the lower sensor, the upper sensor or both of them. There might be a disturbance that affects the upper sensor of dual sphere SGs more than the lower one, for instance, the afore mentioned changes of the vertical alignment, if the tilt compensation is turned on. In that case, one sensor is kept as close as possible to its so-called "tilt nose" (for the definition of "tilt nose" see Appendix E). By convention, this is the lower sensor, and the tilt effects of the lower sensor are limited to frequencies quicker than the response of the tilt compensation. If the two sensors are not perfectly aligned, changes in the vertical alignment at longer time scales can still occur for the upper sensor. In that case, single sphere SGs would be less affected by the disturbance. An analysis of sensor differences of colocated single sphere SGs yields further insights.

Table 4

SGs at the J9 observatory. The table gives the time periods and the data sources used in this study

Instrument	Time period	Data source
st026	2016/02–2018/10	IGETS Level 1 https://doi.org/10.5880/igets.st.l1.001
st023	2016/02–2023/07	IGETS Level 1 https://doi.org/10.5880/igets.st.l1.001
iGrav29	2016/08–2023/07	Personal data set provided by Severine Rosat

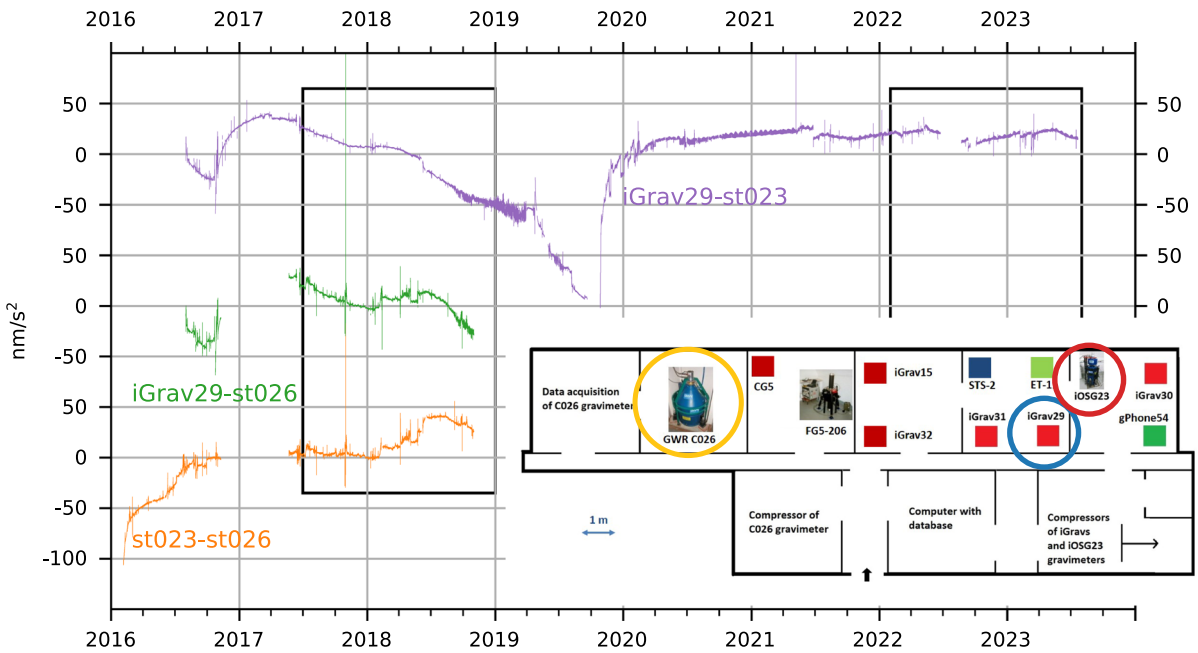

Figure 7

Instrument differences at J9 observatory. The figure shows the differences of three colocated SGs at J9 observatory in Strasbourg. Offsets are adjusted for illustration purposes. Some parts of the signals can be explained by two reinitialisations of iGrav 29 in October 2016 and October 2019. Further, there was much work done on this instrument in July 2017 and a remote test by the manufacturer was performed in April 2019. A closer view of the time window marked with a rectangle can be found in Fig. 8. The plan shows the locations of the instruments, courtesy of S. Rosat

Table 5

SGs at the J9 observatory. Correction of steps and removal of a linear trend

Instrument	# corrected steps	Time period used for estimating a linear trend	trend in nm/(s^2 year)
st026	7	No trend removed	–
st023	5	Full data	9.20
iGrav29	7	No trend removed	–

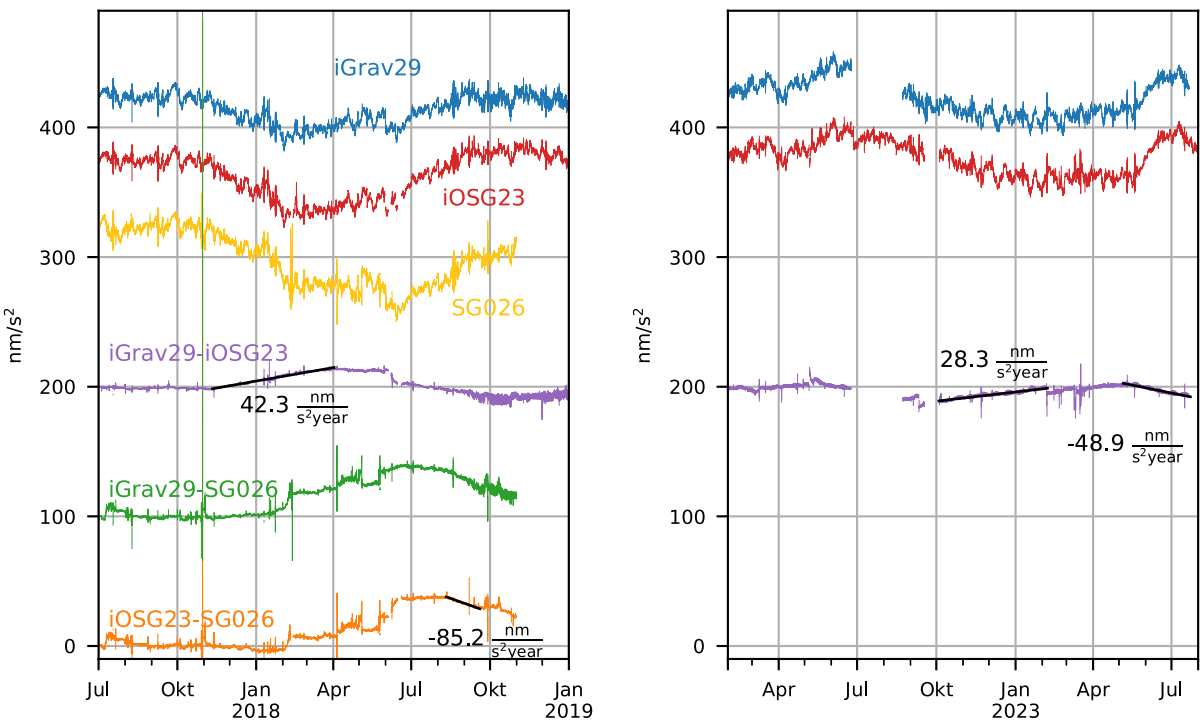

Figure 8

Examples of drift rate changes in instrument differences at J9 observatory. Together with the instrument differences, we show the gravity residuals of the three instruments. To prepare the left plot, the linear trend of iGrav29 is removed for this time period. Offsets are adjusted for illustration purposes

Here, we use data from three SGs at the J9 observatory in Strasbourg: st026, st023 and iGrav29. The operating times and the data sources can be found in Table 4. Figure 7 shows a plan of the location of the instruments inside the observatory building. The data processing is the same as described in Sect. 2. Table 5 gives the number of corrected steps, the time periods used for estimating linear trends and the corresponding trends.

Figure 7 shows the resulting instrument differences. Some parts of the difference signals are linked to work done on iGrav 29, mainly two reinitialisations in October 2016 and October 2019. Further, there was much work done on the instrument in July 2017, and a remote test by the manufacturer was performed in April 2019 (Hinderer et al., 2022)(S. Rosat, 2023, pers. comm.). However, outside of these time periods, we find similar drift rate changes as we found for dual sphere SGs. Examples are shown in Fig. 8.

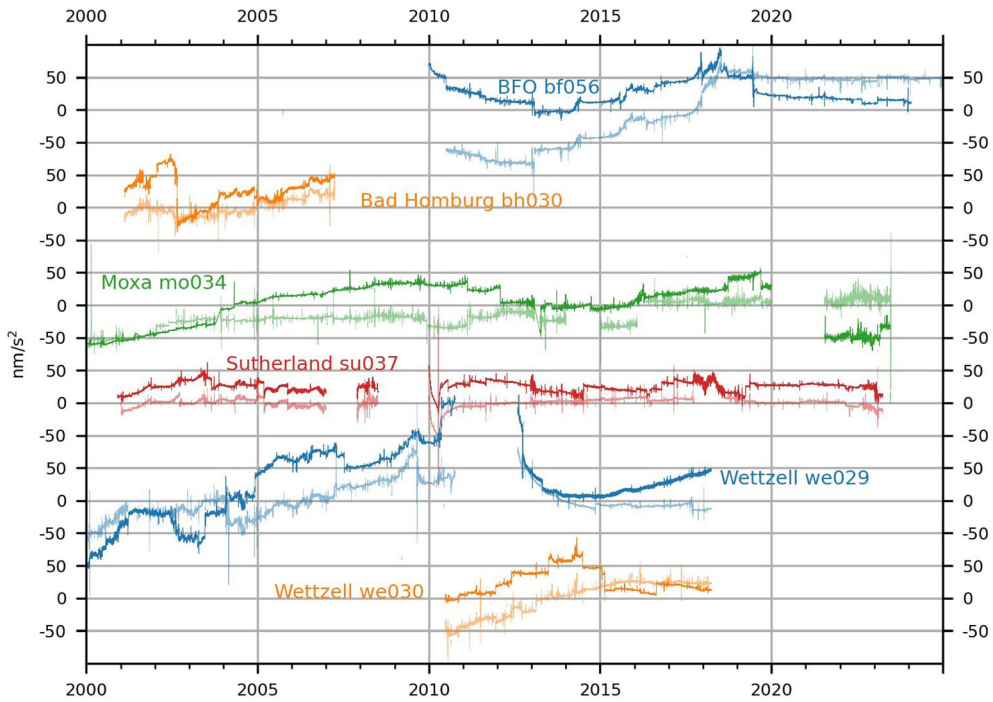

Figure 9
Sensor differences from IGETS Level 2 data. The figure shows the resulting sensor differences from IGETS Level 2 data. The transparent lines in the background show the results from IGETS Level 1 data, calculated in the main part of the paper. Remaining outliers that exceed 150 nm/s^2 are excluded. Offsets are adjusted for illustration purposes

5. *Conclusion*

In the analysis of sensor differences of six dual sphere SGs, we could find signals that are more complicated than linear or exponential drift and steps. These disturbances appear as changes in the drift rate of 20 nm/(s^{2}year) to 83 nm/(s^{2}year) that last several months. Afterwards, the drift rate returns to its previous value. The cumulative signal of one drift rate change is between 5 nm/s^2 and 60 nm/s^2. The return to the old drift rate in most cases coincides with a step in the data. These signals give a lower bound for the disturbance of at least one sensor. Common mode disturbances can be much larger as they cancel out in the sensor difference.

The disturbances cannot be identified in the data of only one sensor. The amplitudes of the drift rate changes are very likely too big to originate from local gravity gradients. Therefore, we expect them to show instrumental effects. The origin of the disturbances is not yet understood. So, they cannot be corrected from the SG time series. The analysis of sensor differences of colocated SGs at the J9 observatory in Strasbourg indicates that similar disturbances exist also for single sphere SGs. In most cases, where only one single sphere SG is located at a measurement site, such disturbances would remain unnoticed because their amplitude and signal character are similar to the gravity variation of natural origin.

The disturbances are at the level of half of the amplitude of the gravity residuals themselves and might lead to misinterpretation of the gravity residuals. As the disturbances occur on time scales of several months, they should not affect the analysis of short-period signals like normal mode seismology or tidal analysis in the diurnal or semi-diurnal band. To be aware of the characteristics and size of the disturbances is important if gravity changes of a few tens of nm/s^2 are studied on time scales longer than months. Examples are signals from hydrology with typical amplitudes of 80 nm/s^2 to 180 nm/s^2 or polar motion with an amplitude of up to 40 nm/s^2.

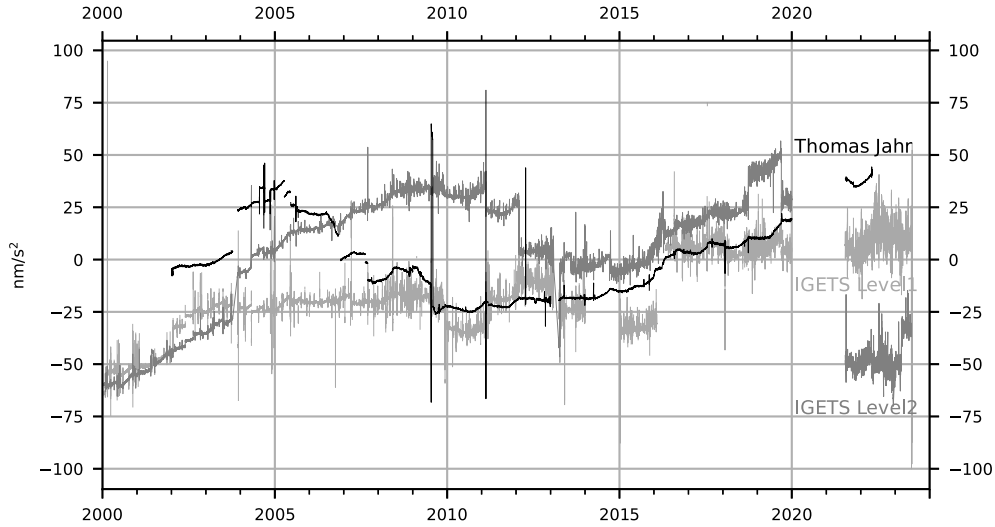

Figure 10
Sensor differences of the instrument mo034 at Moxa calculated from different data sets. The figure shows the resulting sensor differences from IGETS Level 1 data, IGETS Level 2 data and a data set provided by the operators (Thomas Jahr). Remaining outliers that exceed 100 nm/s^2 are excluded. Offsets are adjusted for illustration purposes

Acknowledgements

Thanks to Severine Rosat for providing the data of the iGrav29 at the J9 observatory in Strasbourg and sharing details about the operation of the gravimeters in Strasbourg. We further thank Thomas Jahr for providing the dataset of the mo034 gravimeter in Moxa after outlier rejection and step correction. Thank you to the reviewers for the well-considered comments, that helped to improve the manuscript. We acknowledge the fruitful discussion with Walter Zürn and Rudolf Widmer-Schnidrig. Thank you to Thomas Götz for helping with the preparation of Fig. 1.

Author Contributions C.B. conducted the analyses. T.F. and N.S. have advised on the work. C.B. prepared the manuscript. All authors discussed the results and reviewed the manuscript.

Funding

Open Access funding enabled and organized by Projekt DEAL. The authors declare that no funds, grants, or other support were received during the preparation of this manuscript.

Data Availability

Data of iGrav29 at the J9 observatory in Strasbourg was provided by Severine Rosat. A dataset of the mo034 gravimeter in Moxa after outlier rejection and step correction was provided by Thomas Jahr. The data of environmental and instrumental parameters of the instrument bf056 are available on request to the authors. All other SG gravity data sets used in this study are freely available from the data bank provided by IGETS (Boy et al., 2023).

Declarations

Conflict of interest The authors declare no Conflict of interest.

Appendix A: Outlier Rejection

This is a detailed description of the outlier rejection used in Sect. 2. For each data point of the gravity residuals the median $\tilde{g}^{\mathrm{res}}$ in a one-week window is determined. The current data point g_i^{res} lies in the middle of this window. Afterwards the median of the absolute deviations MAD from $\tilde{g}^{\mathrm{res}}$ is calculated in the same window:

$$\mathrm{MAD} = \mathrm{median}(|g_i^{\mathrm{res}} - \tilde{g}^{\mathrm{res}}|)\,.$$

It is further scaled to make it consistent with the standard deviation for normally distributed data (Ruppert and Matteson, 2015):

$$\mathrm{SMAD} = 1.483 \cdot \mathrm{MAD}\,,$$

where SMAD is the scaled median absolute deviation. We define g_i^{res} as an outlier if

$$|g_i^{\mathrm{res}} - \tilde{g}^{\mathrm{res}}| > 5 \cdot \mathrm{SMAD}\,.$$

Appendix B: Sensor Differences From Alternative Data Sets

In the main part of the paper, we calculate sensor differences from IGETS Level 1 data as described in Sect. 2. To ensure the drift rate changes we find are not artefacts of our data processing, here we calculate sensor differences from IGETS Level 2 products (Boy, 2022) processed by EOST (École et observatoire des sciences de la terre). In these datasets voltage is already converted to gravity and instrumental disturbances like steps and outliers are corrected. We compute gravity residuals as described in Sect. 2. The conversion from voltage to gravity, the step and the outlier correction are not needed here. As the tidal correction and the air pressure correction are the same for both sensors, the sensor difference is equivalent to the difference between the Level 2 data of both sensors. The results are shown in Fig. 9.

For the instrument mo034 in Moxa, we additionally compute the sensor difference from a data set provided by the operators after outlier and step correction (T. Jahr, 2022, pers. comm.). In contrast to the IGETS Level 1 and Level 2 data, this data set has a lower sampling rate of one hour. A comparison of all sensor differences calculated for the instrument mo034 can be seen in Fig. 10.

While the remaining steps and the presence of high-frequency noise differ between the sensor differences computed from different data sets, the drift rate changes remain unchanged. For the instrument mo034 in Moxa, a new drift rate change appears between August 2015 and August 2016, a time period where the Level 1 data set has a gap. The cumulative signal of this drift rate change is 20 nm/s^2. This is larger than the drift rate change of this instrument found in the main part of the paper.

Appendix C: Modelling the Effect of Local Masses on the Gravity Gradient

In this section, we reproduce a gravity difference of 20 nm/s^2 between the two sensors of a dual sphere SG with cylinders of different size as a simple model of local masses.

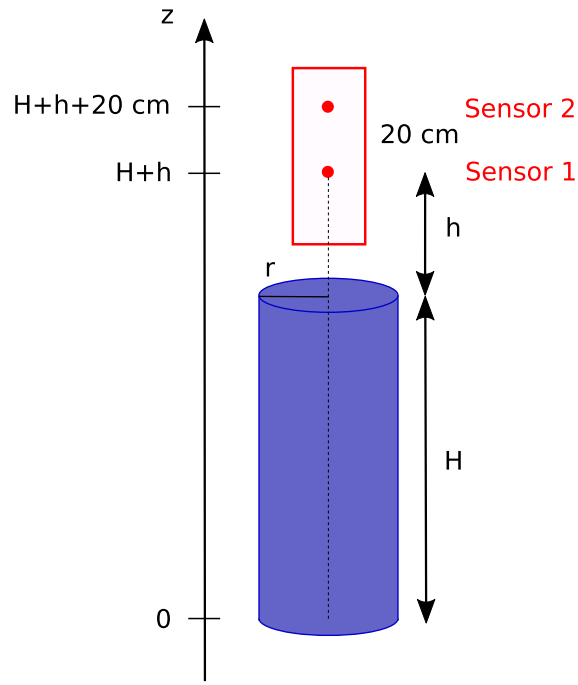

Figure 11
Cylinder below the gravimeter. The figure shows the geometry of the cylinder used to reproduce a gravity difference of 20 nm/s^2 between the two sensors. For different values of H, h and r we calculate the needed density of the cylinder

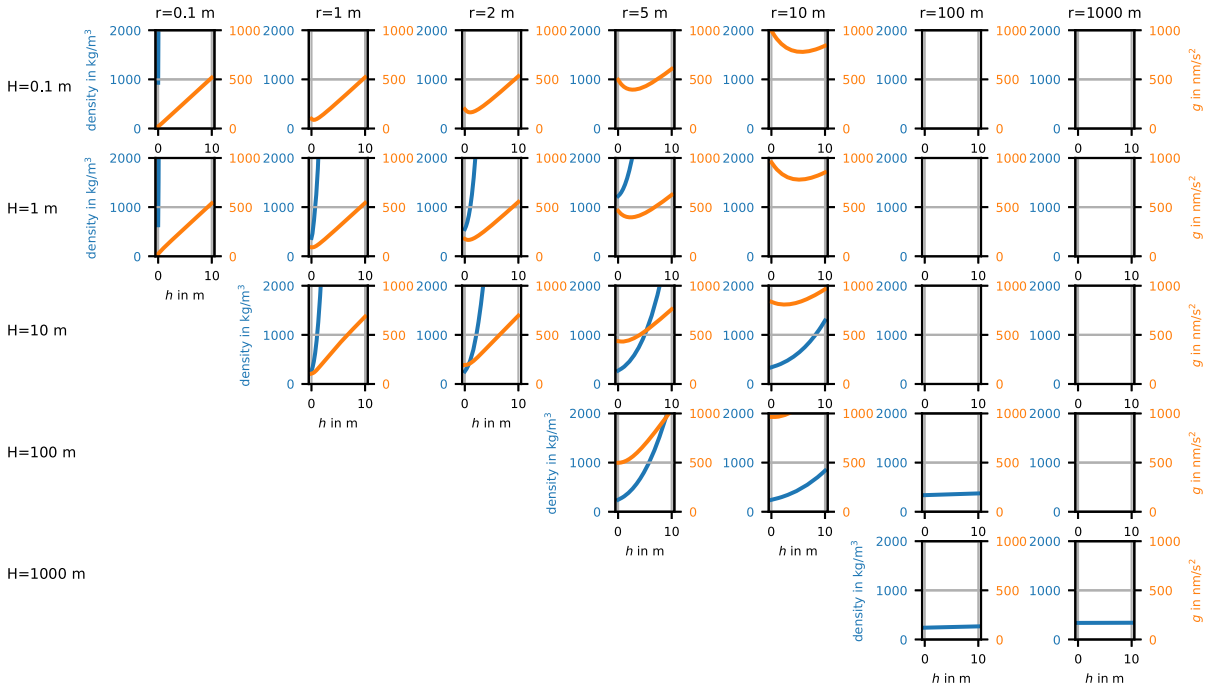

Figure 12

Sensor differences induced by a cylinder of height H, radius r, and distance h to the gravimeter (see Fig. 11). We vary the distance h to the gravimeter and calculate the density (left scale, blue) needed to generate a sensor difference of 20 nm/s^2. Further, we calculate the corresponding total gravity effect (right scale, orange) of the cylinder at the location of the lower sensor. Results for the density are only shown if they are smaller than 2000 kg/m^3, results for the gravity effect are only shown if they are smaller than 1000 nm/s^2. Especially for large radii ($r \geq 100$m), it may therefore be the case that no density or no gravitational effect is shown because all the values are larger than these thresholds

We place a homogeneous cylinder of height H and a radius r below the gravimeter. The cylinder axis coincides with the sensor axis. The cylinders upper bound has a distance of h to the lower sensor of the gravimeter (see Fig. 11). The gravity effect

$$g = -2\pi G\rho\left(-H + \sqrt{r^2+z^2} - \sqrt{r^2+(z-H)^2}\right) \tag{C1}$$

of such a cylinder with density ρ at a location z above its bottom (see Fig. 11) is given by Hofmann-Wellenhof and Moritz (2006).

The locations of the sensors are $z_1 = H + h$ and $z_2 = H + h + \delta z$, where $\delta z = 20$cm is the distance between the sensors. This leads to a gravity difference of

$$\Delta g = -2\pi G\rho \left(\left(\sqrt{r^2+(H+h)^2} - \sqrt{r^2+h^2} - \sqrt{r^2+(H+h+\delta z)^2} + \sqrt{r^2+(h+\delta z)^2}\right)\right)$$

between the two sensors. Hence,

$$\rho = -\frac{\Delta g}{2\pi G}\frac{1}{\sqrt{r^2+(H+h)^2} - \sqrt{r^2+h^2} - \sqrt{r^2+(H+h+\delta z)^2} + \sqrt{r^2+(h+\delta z)^2}} \tag{C2}$$

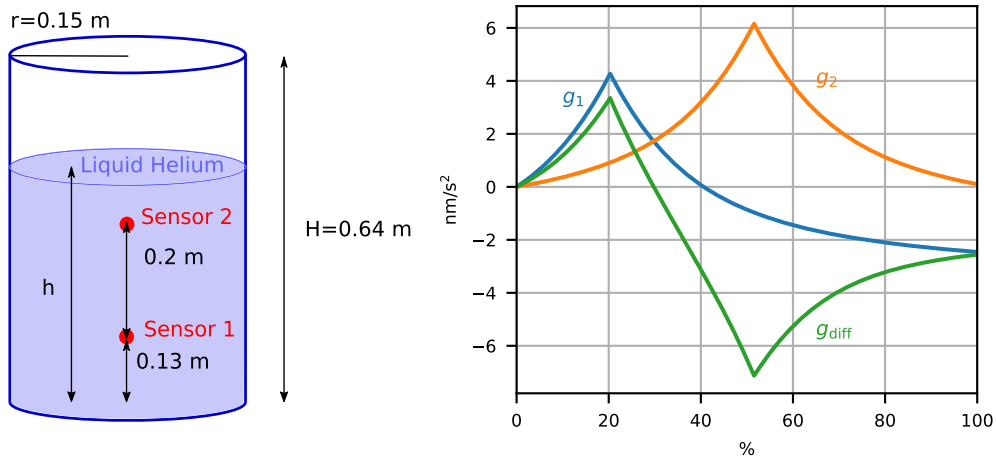

Figure 13
Modelling the gravity effect of variations of the liquid helium level. The geometry of the model is shown on the left. The figure on the right shows the gravity changes g_1 and g_2 at the upper and the lower sensors originating from the liquid helium level. g_{diff} shows the resulting sensor difference

is the density needed to cause the difference Δg at the given geometry r, H, h, and δz.

For different radius r and height H of the cylinder, we vary the distance h to the gravimeter and compute the density needed to cause a gravity difference of 20 nm/s^2 between the two sensors. Figure 12 shows the results. Additionally, we compute the total gravity effect at the location $z_1 = H + h$ of the lower sensor with Eq. (C1) and show the results in Fig. 12. We excluded those cylinders where the height of the cylinder is much larger than the radius of the cylinder, as we can hardly imagine a corresponding geophysical process.

For the very small cylinders ($r < 1$ m), the distance to the gravimeter has to be extremely small to let the needed change in density not be unrealistically large. For a cylinder of height $H = 1$ cm and a radius $r = 1$ cm, the needed density already reaches values larger than the density of water, if the distance to the lower sensor is larger than 1 cm. For all tested cylinders with a radius larger than 2 m, the corresponding gravity change at the lower sensor becomes significantly larger than the variations of the gravity residuals observed in Fig. 4. Further, the needed density change gets extremely large for all cylinders where $r \gg H$. In these cases, the cylinder approaches a Bouguer plate, for which the gravity gradient vanishes independent of density.

The only test cases for which the needed change in density falls into a realistic range and where the resulting change in total gravity is on the observed order of magnitude ($\leq 200\, nm/s^2$, see Fig. 3) are cylinders with a radius of 1 m or 2 m and a height of at least 1 m. However, also in these cases, the cylinder has to be very close to the gravimeter ($h < 1$m).

Appendix D: Gravity Effect of Varying Liquid Helium Level

To assess a possible variation of the sensor difference due to fluctuations in the liquid helium level, we model the gravity effect of the liquid helium for both sensors.

We model the inner part of the Dewar, which is filled with helium, as a cylinder with a diameter of 0.3 m and a height of $H = 0.64$ m (see Fig. 13). The geometry was provided by R. J. Warburton and R. C. Reinemann (pers. comm.). The gravity effect of a liquid helium cylinder of the same diameter and height h is calculated for the two sensors at $z_1 = 0.13$ cm and $z_2 = 0.33$ cm. h varies between $0\%H$ and $100\%H$. The density of liquid helium at 4.2 K is 125 kg/m^3 (Berman and Mate, 1958). For $h \leq z$ the gravity effect of the liquid helium cylinder can

directly be calculated by Eq. C1. For $h > z$, we divide the liquid helium cylinder into two parts, one above the sensor and one below. We add up the two gravity effects. The results and the difference between the two sensors are shown in Fig. 13. The maximum variation of the sensor difference occurs between a helium level of 20 % and 51 %. It is 10.5 nm/s^2. For some dual sphere SGs, this is at the same order of magnitude as the observed variations of sensor differences. However, for the example of BFO, liquid helium level variations are only between 90 % and 100 %, which leads to variations in the sensor difference of less than 2 nm/s^2. Liquid helium level variations might be larger for older SGs without an ultra-long hold time Dewar and a corresponding efficient cold head.

This model gives an upper limit for the gravity effect of liquid helium level variations. In reality, the two sensors are not floating in liquid helium, but are built inside the gravity sensing unit, which has its own volume not filled with liquid helium.

Appendix E: Variations of the Sensor Difference Due to Tilt

In this section, we examine whether the observed signals in the sensor difference can be related to changes in the vertical alignment of the sensors. We do this for the example of the instrument bf056 where the tilt compensation system is turned off. Manual checks of the vertical alignment were performed on January 30, 2013, and September, 23, 2020. From the results of these tests, we calculate the vertical alignment of the two sensors on these two dates. This change in alignment should cause a change in sensor difference. We compare this change between the two dates with the actual variation of the sensor difference presented in Fig. 3.

Opposite to spring gravimeters, tilts of SGs increase the measured gravity value. For small tilt angles, this behaviour follows a parabola. One possibility to check the verticality is to apply the same tilt in opposite directions. If the sensitive direction of the instrument is aligned with gravity, the resulting change in the output values should be the same. In that case, we say that the instrument is "operated at its tilt nose". The check of the vertical alignment is performed in two orthogonal directions.

Figure 14 shows a sketch of the measurements on the tilt parabola during the test. As only gravity differences are measured, for simplicity, we set the measured gravity for perfect vertical alignment to zero. Then the parabola takes the form

$$g(h) = ah^2\,,$$

where g is the gravity measurement, h is the vertical alignment and a is the dilatation parameter of the parabola. The measurement starts at h_0 and

$$g_0 = ah_0^2\,. \tag{E3}$$

By applying the same tilt Δh in opposite directions, we measure the corresponding changes in gravity

$$\Delta g^+ = a\,(h_0 + \Delta h)^2 - g_0 = a\,(h_0^2 + 2h_0\Delta h + \Delta h^2) - g_0 \tag{E4}$$

and

$$\Delta g^- = a\,(h_0 - \Delta h)^2 - g_0 = a\,(h_0^2 - 2h_0\Delta h + \Delta h^2) - g_0\,. \tag{E5}$$

From Equations (E3), (E4) and (E5) we can obtain

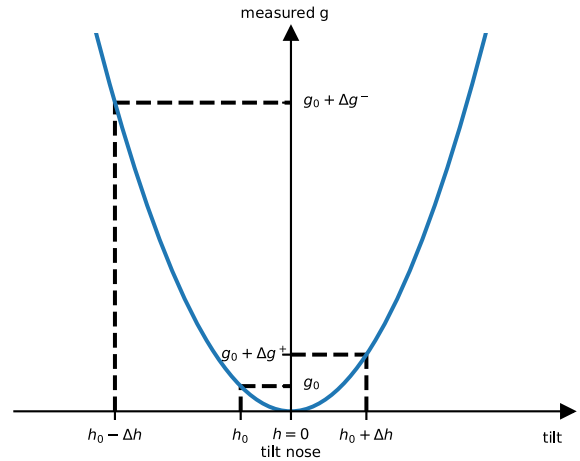

Figure 14
Test of vertical alignment. Before the test the gravimeter is operated at vertical alignment h_0. The measured gravity value is g_0. Then the tilt Δh is applied in positive and negative directions, and the gravity changes Δg^- and Δg^+ are measured. As only gravity changes are measured, for simplicity, we set the measured gravity for perfect vertical alignment to zero

Table 6

Test of the vertical alignment of the sensors at BFO. The table gives the results of the tests and the resulting gravity effects. h_X and h_Y are the values of the vertical alignment h_0 for the two directions

	30.01.2013		23.09.2020	
	lower sensor	upper sensor	lower sensor	upper sensor
a_X in nm/(s^{2}µrad^2)	1.31 10^{-2}	1.35 10^{-2}	1.21 10^{-2}	1.43 10^{-2}
a_Y in nm/(s^{2}µrad^2)	1.35 10^{-2}	1.54 10^{-2}	1.21 10^{-2}	1.50 10^{-2}
h_X in µrad	− 3.16 ± 0.29	− 16.79 ± 1.51	− 23.25 ± 2.09	− 40.59 ± 3.65
h_Y in µrad	− 1.24 ± 0.11	13.07 ± 1.18	0.41 ± 0.04	15.69 ± 1.41
g_{tilt} in nm/s^2	0.16 ± 0.03	6.17 ± 0.98	7.37 ± 1.48	25.79 ± 4.69
sensor difference nm/s^2	− 6.01 ± 0.97		− 18.42 ± 4.60	

$$a = \frac{\Delta g^+ + \Delta g^-}{2\Delta h^2}$$

and

$$h_0 = \frac{\Delta g^+ - \Delta g^-}{4a\Delta h}\,.$$

We calculate a for the two orthogonal directions X and Y for both sensors and both measurements. The results are listed in Table 6. In the following, we assume a to be the same for both directions, both sensors and both dates. This might not be completely true. a could, for example, be different for different directions due to imperfect symmetry of the sensors or change with time due to deformation of the sensors. A measure of the size of possible changes is given by the variation of the values of a given in Table 6. In the following, we use the mean value of a and choose its standard deviation as a measure of the error we make by assuming a to be constant: $a = (1.36 \pm 0.12) \times 10^{-2}\text{nm}/(\text{s}^2\mu\text{rad}^2)$. Further, we calculate h_0 for each sensor and direction. They are called h_X and h_Y in the following. The results can be found in Table 6. h_X and h_Y give the angle between the "tilt nose" and the actual directions of the sensors. A change in h_X or h_Y can either be caused by a tilt of the sensor or by a change in the position of the "tilt nose".

As the parameter a is assumed to be the same in both directions, the parabola in 3D can be expressed by

$$g_{\text{tilt}} = a(h_X^2 + h_Y^2)\,.$$

For both dates, g_{tilt} for both sensors and the resulting sensor difference is calculated. The results are given in Table 6. We find that due to the changes in vertical alignment between January 30, 2013, and September, 23, 2020, the sensor difference should have changed by about 12.4± 5.0 nm/s^2. In comparison, the observed change in sensor difference between these two dates is 105 nm/s^2 (see Fig. 3).

Appendix F: Operator interventions during time periods of changed drift rate

In the following for each instrument we list some details about operator interventions during time periods of changed drift rate. For instrument bf056 they are taken from local log-files and the handwritten instrument book. For the other instruments the log-files provided together with the IGETS level 1 data are used.

bf056, Schiltach, BFO

- On May 12, 2014, about two months after the beginning of a time period of changed drift rate (starting in March 2014, see Fig. 6) the uninterruptible power supply was tested. This caused an unintended failure of the compressor and the cold head and apparently caused a step in the data.
- The return to the old drift rates on June 5, 2014, is in coincidence with a power outage, a cleaning of the cold head and a step in the data.
- During the time period of the changed drift rate in 2017/18, the gravity data of the upper sensor shows a higher noise level at high frequencies. Contrary to the changed drift rate, this was realized at the

time by the operators. In search for the cause, tests were carried out like opening the door of the SG chamber or touching the cold head. The return to the old drift rate is in coincidence with a change of the gravity control card of the upper sensor on July 13, 2018. At the same time, there is a step in the gravity data of the lower sensor, and the high frequency noise of the upper sensor reduces.

bh030, Bad Homburg

- Some of the steps in the sensor difference of the instrument bh030, which might be responsible for the apparent drift rate change coincides with tests of the step response of the upper sensor on May 22, May 31 and July 5, 2006, and helium refill and ice removal on May 31, 2006.

mo034, Moxa

- The onset of the drift rate change in Moxa coincides with a strong increase in groundwater level on May 20, 2019. However, as discussed in Sect. 4.2, we do not expect it to be the reason for the drift rate change.
- During the time of the changed drift rate in July 2019 several problems and operator interventions occurred: helium gas was refilled into the compressor, the water cooler was refilled and the compressor was restarted twice, once after a thunderstorm and again due to problems.
- The return to the old drift rate on September 12, 2019 coincides with the refill of helium and a step in the data.

su037, Sutherland

- From December 2001 on the there sometimes occur gaps (around one in three months) in the auxiliary data. These gaps become more frequent (around ten per month) in January 2003, additionally short data gaps in the gravity data occur. From January 2003, reinstallations of electronic components and power cycles were carried out in search of a solution. The problem could not be solved until the end of 2003. Afterwards, no log-files for the instrument are provided on IGETS any more until December 2007. At that time, the problem was solved.
- All periods of changed drift rate we found for the instrument su037 fall into the time of the described problems of the data acquisition.
- Two data gaps in the auxiliary data occurred in September 2002, shortly before the end of the first time period with a changed drift rate (June 1, 2002 to September 23, 2002).
- The second time period of changed drift rate (February 17, 2003 to June 8, 2003) falls into the time of intensive search for a solution to the data acquisition problems.
- For both examples of changed drift rate, the return to the old drift value coincides with a helium refill.

we029, Wettzell

- For the instrument we029 in Wettzell, noise from a defective cold head occurred in the period of changed drift rate. The problems of the cold head became more severe from June 18, 2003, on. It was removed on June 23. The removal of the cold head coincides with the return to the old drift rate. Helium was refilled on the day after, and ice was removed. The gravimeter was without a cold head for one week. On June 30, 2006, the cold head was inserted again after repair. We can not see an effect of the operation without a cold head in the residuals or the sensor difference.

we030, Wettzell

- The period of changed drift rate of the instrument we030 starts in December 2011. Ice occurred in the neck of the cold head after a power failure on March 20, 2012. It was cleaned on March 23, and the cold head was centred on March 27.

- The drift returned to its old value on May 31, 2012. On the same day, ice was again present in the neck of the cold head. The ice was removed later on June 19, 2012.

References

Berman, R., & Mate, C. F. (1958). Some thermal properties of helium and their relation to the temperature scale. *The Philosophical Magazine: A Journal of Theoretical Experimental and Applied Physics, 3*(29), 461–469. https://doi.org/10.1080/14786435808244568

Boy, J.-P. (2022). Description of the Level 2 and Level 3 IGETS data produced by EOST (Version 2). https://isdc.gfz-potsdam.de/fileadmin/isdc/docs/EOSTproducts_v2.pdf

Boy, J.-P., Barriot, J.-P., Förste, C., Voigt, C., & Wziontek, H. (2023). Achievements of the first 4 years of the international geodynamics and earth tide service (IGETS) 2015–2019. In J. T. Freymueller & L. Sánchez (Eds.), *Beyond 100: The Next Century in Geodesy* (pp. 107–112). Cham: Springer.

Bützler, C. (2018). Drift des supraleitenden Gravimeters SG056 am BFO. Bachelorarbeit, Karlsruher Institut für Technologie. https://doi.org/10.5445/IR/1000082191

Carbone, D., Cannavò, F., Greco, F., Reineman, R., & Warburton, R. J. (2019). The benefits of using a network of superconducting gravimeters to monitor and study active volcanoes. *Journal of Geophysical Research: Solid Earth, 124*(4), 4035–4050. https://doi.org/10.1029/2018JB017204

Creutzfeldt, B., Güntner, A., Thoss, H., Merz, B., & Wziontek, H. (2010). Measuring the effect of local water storage changes on in situ gravity observations: Case study of the geodetic observatory Wettzell. *Germany. Water Resources Research,46*(8). https://doi.org/10.1029/2009WR008359

Crossley, D., Hinderer, J., & Riccardi, U. (2013). The measurement of surface gravity. *Reports on progress in physics,76*(046101). https://doi.org/10.1088/0034-4885/76/4/046101

Crossley, D., Hinderer, J., & Boy, J.-P. (2004). Regional gravity variations in Europe from superconducting gravimeters. *Journal of Geodynamics, 38*(3), 325–342. https://doi.org/10.1016/j.jog.2004.07.014

Dehant, V., Defraigne, P., & Wahr, J. M. (1999). Tides for a convective earth. *Journal of Geophysical Research: Solid Earth, 104*(B1), 1035–1058. https://doi.org/10.1029/1998JB900051

Ding, H., & Chao, B. J. (2017). Solid pole tide in global GPS and superconducting gravimeter observations: Signal retrieval and inference for mantle anelasticity. *Earth and Planetary Science Letters, 459*, 7244–7251. https://doi.org/10.1016/j.epsl.2016.11.039

Goodkind, J. M. (1999). The superconducting gravimeter. *Review of Scientific Instruments, 70*(11), 4131–4151. https://doi.org/10.1063/1.1150092

Hinderer, J., Crossley, D., & Warburton, R. J. (2007). Gravimetric methods – superconducting gravity meters. In: Schubert, G. (ed.) Treatise on Geophysics vol. 10, pp. 65–122. Elsevier, Oxford. Chap. 3.04

Hinderer, J., Rosat, S., Crossley, D., Amalvict, M., Boy, J.-P., & Gegout, P. (2002). Influence of different processing methods on the retrieval of gravity signals from GGP data. *Bulletin d'informations des Marées Terrestres, 123*, 9278–9301.

Hinderer, J., Warburton, R. J., Rosat, S., Riccardi, U., Boy, J.-P., Forster, F., Jousset, P., Güntner, A., Erbas, K., Littel, F., & Bernard, J.-D. (2022). Intercomparing superconducting gravimeter records in a dense meter-scale network at the J9 gravimetric observatory of Strasbourg, France. *Pure and Applied Geophysics, 179*, 1701–1727. https://doi.org/10.1007/s00024-022-03000-4

Hofmann-Wellenhof, B., & Moritz, H. (2006) Physical Geodesy. Springer, Vienna. https://doi.org/10.1007/978-3-211-33545-1

Instruments, G. W. R. (2009). *Operators Manual Superconducting Gravimeter Serial Number: DSG-056*. US: San Diego.

Kroner, C., Dierks, O., Neumeyer, J., & Wilmes, H. (2005). Analysis of observations with dual sensor superconducting gravimeters. *Physics of the Earth and Planetary Interiors, 153*(4), 210–219. https://doi.org/10.1016/j.pepi.2005.07.002

Kumar, S., Rosat, S., Hinderer, J., Mouyen, M., Boy, J.-P., & Israil, M. (2023). Delineation of aquifer boundary by two vertical superconducting gravimeters in a karst hydrosystem, France. *Pure and Applied Geophysics, 180*, 611–628. https://doi.org/10.1007/s00024-022-03186-7

Luan, W., Shen, W., & Jia, J. (2023). Analysis of iGrav superconducting gravity measurements in Kunming, China, with emphasis on calibration, tides, and hydrology. *Pure and Applied Geophysics, 180*, 643–660. https://doi.org/10.1007/s00024-022-03036-6

Neumeyer, J., Barthelmes, F., Kroner, C., Petrovic, S., Schmidt, R., Virtanen, H., & Wilmes, H. (2008). Analysis of gravity field variations derived from superconducting gravimeter recordings, the GRACE satellite and hydrological models at selected European sites. *Earth, Planets and Space, 60*, 505–518. https://doi.org/10.1186/BF03352817

Pagiatakis, S. D. (2000). Application of the least-squares spectral analysis to superconducting gravimeter data treatment and analysis. *Bulletin d'informations des Marées Terrestres, 113*, 10415–10425.

Richter, B. (1998). A new generation of superconducting gravimeters. In: Proc. of the 13th Int. Symp. on Earth Tides, pp. 545–555. Observatoire Royal de Belgique, Série Géophysique, Brussels

Ruppert, D., & Matteson, D. S. (2015). Statistics and Data Analysis for Financial Engineering. Springer, New York. https://doi.org/10.1007/978-1-4939-2614-5

Van Camp, M., & Francis, O. (2007). Is the instrumental drift of superconducting gravimeters a linear or exponential function of time? *Journal of Geodesy, 81*, 337–344. https://doi.org/10.1007/s00190-006-0110-4

Van Camp, M., & Vauterin, P. (2005). Tsoft: graphical and interactive software for the analysis of time series and Earth tides. *Computers & Geosience, 31*, 631–640. https://doi.org/10.1016/j.cageo.2004.11.015

Wziontek, H., Falk, R., Wilmes, H., & Wolf, P. (2009). Precise gravity time series and instrumental properties from combination of superconducting and absolute gravity measurements. In M. G. Sideris (Ed.), *Observing Our Changing Earth* (pp. 301–306). Berlin, Heidelberg: Springer.

Xu, J.-Q., Sun, H.-P., & Yang, X.-F. (2004). A study of gravity variations caused by polar motion using superconducting gravimeter data from the GGP network. *Journal of Geodesy, 78*, 201–209. https://doi.org/10.1007/s00190-004-0386-1

Ziegler, Y., Hinderer, J., Rogister, Y., & Rosat, S. (2016). Estimation of the gravimetric pole tide by stacking long time-series of GGP superconducting gravimeters. *Geophysical Journal International, 205*, 77–88. https://doi.org/10.1093/gji/ggw007

(Received June 18, 2025, revised November 27, 2025, accepted December 14, 2025)